Optics Letters

Amplification of mid-IR continuum for broadband 2D IR spectroscopy

John H. Hack, Nicholas H. C. Lewis, William B. Carpenter,† and Andrei Tokmakoff*

Department of Chemistry, the James Franck Institute and the Institute for Biophysical Dynamics, University of Chicago, 929 E 57th Street, Chicago, Illinois 60637, USA
**Corresponding author: tokmakoff@uchicago.edu*
†Current address: Department of Chemistry, Stanford University, Stanford, California 94305, USA

Received 21 November 2022; revised 29 December 2022; accepted 11 January 2023; posted 11 January 2023; published 8 February 2023

We report the generation and characterization of microjoule level, broad bandwidth femtosecond pulses in the mid-infrared (MIR) using optical parametric amplification of continuum MIR seed pulses in GaSe. The signal (3 μm) and idler (6 μm) pulses have energies of 6 μJ and 3 μJ with bandwidths of ~950 cm^{-1} and 650 cm^{-1} FWHM and pulse lengths of 34 fs and 80 fs. Broadband 2D IR spectra of O-H and N-H transitions are acquired with the signal beam demonstrating the capabilities of this source for cross peak and line shape measurements.

https://doi.org/10.1364/OL.481088

The generation of few-cycle IR pulses has advanced rapidly in recent years, with applications in high-harmonic generation [1], terahertz generation [2], solid-state physics [3], and infrared spectroscopy [4]. While all operating in the mid-IR (MIR) spectral range, these various applications have different design and implementation requirements for pulse energy, spectrum, bandwidth, and compression, and a wide range of generation strategies have been tailored to different needs [5]. For ultrafast IR spectroscopy, design criteria include compression at the sample, broad bandwidth, and smoothly varying spectrum for spectral coverage, microjoule pulse energies to excite molecular vibrations, and shot-to-shot stability for averaging. Increasing pulse bandwidth—and thus spectral coverage—while meeting all other requirements would dramatically improve capabilities for measuring broad vibrational line shapes, simultaneous measurement of multiple transitions, and data collection efficiency. Major practical challenges include generating suitable pulses and delivering compressed pulses to the sample through the transmissive optics required in experiments for interferometry and sample housing. While often manageable for narrower pulses, the temporal and spatial dispersion accumulated from transmissive optics increases with pulse bandwidth. Dispersion compensation is more difficult in the MIR than in the visible, as chirp mirrors are unavailable and prism or grating compressors are lossy and difficult to align.

Ultrafast two-dimensional infrared (2D IR) spectroscopy has been used extensively to measure the vibrational structure and dynamics in molecular systems [6]. In state-of-the-art experiments, microjoule pulse energies are obtained by downconversion via optical parametric amplification (OPA) or difference frequency generation (DFG) on Ti:sapphire systems, with bandwidths limited to 150–400 cm^{-1} and pulse durations of 45–70 fs [4,7–9]. This covers only a fraction of the MIR spectral range of 500–4000 cm^{-1}, making tuning necessary for broad spectral coverage [4,9].

Alternative generation schemes include laser filamentation in gases, which produced pulses with broad, smooth spectra covering the MIR with typical pulse energies of the order of 10–100 nJ [10,11]. These broadband IR (BBIR) continuum sources have been implemented as a probe in 2D IR spectroscopy, dramatically increasing the accessible detection bandwidth [4,9], though pulse energies are too low to excite molecular vibrations. Microjoule pulse energies have been reached via OPA or DFG in non-oxide crystals such as GaSe, $ZnGeP_2$ (ZGP), and $CdSiP_2$ (CSP) which support broad phase-matching when pumped near 2 μm [1,12–14]. A variety of pump sources and repetition rates are used, reaching large power by OPCPA [1,12], lasing near 2 μm in Cr^{2+}:ZnS or Tm-doped systems [15,16], or downconversion from 1-μm lasers [14]. Large average MIR powers were attained by intra-pulse DFG, though pulse energies were submicrojoule at high repetition rates [15,16]. While the generation of extraordinarily short, intense, or broadband IR pulses have been reported [5], suitable pulses which meet all requirements for 2D IR vibrational spectroscopy, while significantly improving on a bandwidth of 400 cm^{-1}, have not yet been demonstrated and implemented in experiments.

In this work, we report the generation and implementation of broadband, microjoule MIR pulses spanning >1000 cm^{-1} for excitation and detection in 2D IR spectroscopy of O-H and N-H molecular vibrations. Because the BBIR source meets all requirements but pulse energy, our strategy is to amplify that pulse by OPA with a 2-μm pump in GaSe, which supports a broader phase-matching bandwidth and transparency range than CSP or ZGP [13]. The OPA and 2D IR apparatuses are designed to minimize transmissive optics, and amplified pulses are compressed at the sample using the bulk material. Based on Ti:sapphire and TOPAS technology, this light source operates on systems readily available in many ultrafast spectroscopy labs.

Figure 1 shows a schematic of the OPA and 2D IR interferometer and spectrometer. The output of a Ti:sapphire regenerative amplifier (Coherent Legend Elite, 25 fs, 1 kHz) is split into two paths: 0.7 mJ is used to generate the seed and 1.8 mJ to

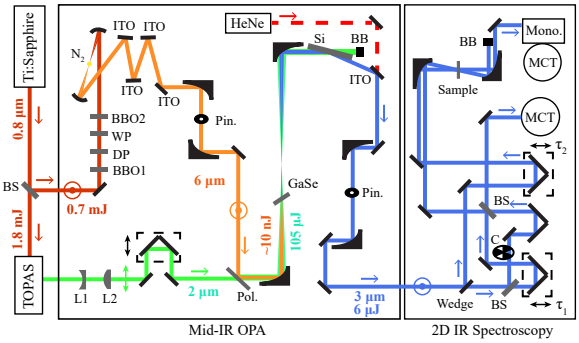

Fig. 1. Mid-IR OPA and 2D IR interferometer and spectrometer. BB, beam block; BBO, β-barium borate; BS, beam splitter; C, optical chopper; DP, delay plate; L, lens; MCT, HgCdTe detector; Mono., monochromator; Pin, pinhole; Pol, polarizer; WP, wave plate. Color scheme: red, Ti:sapphire fundamental; orange, seed; green, pump; blue, signal; dashed red, visible tracer.

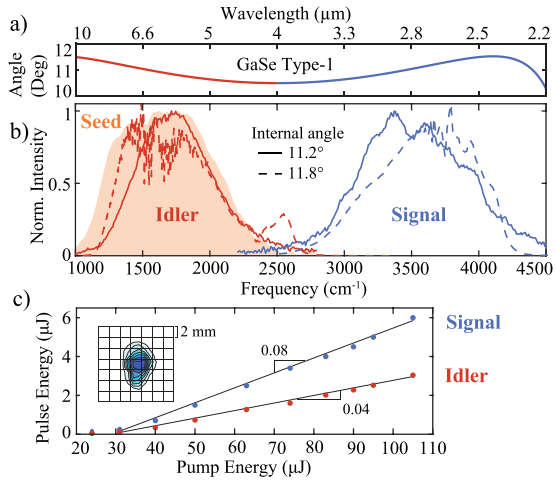

Fig. 2. (a) Type-1 phase matching curve for GaSe pumped at 2 μm. (b) Pulse spectra at phase matching angle 11.2° (solid) and 11.8° (dashed). (c) Pulse energy scaling with linear fit; inset, signal spatial profile.

generate the pump. The 2-μm pump (50 fs, 105 μJ ± 0.5% at the GaSe crystal) is generated as the idler from a commercial OPA (Light Conversion TOPAS Prime) and expanded to a diameter of ~13-mm 1/e^2 with a Galilean telescope.

In the seed line, continuum MIR is generated using a scheme that has been described in detail previously [11]. The 800-nm fundamental and its second and third harmonics are tightly focused into N_2 gas to generate a plasma which radiates light from 2.5 to 10 μm with a spectrum peaked near 6 μm. The generated BBIR is recollimated and separated from the other fields with four consecutive reflections off ITO coated glass (PGO CEC007S). The BBIR is spatially filtered to improve the beam profile and focusing using a 150-μm pinhole at the focus of two bare gold coated 90° off-axis parabolic mirrors (Au-OAP), f = 100 mm, resulting in a 20% improvement in OPA efficiency. The resulting 50-fs BBIR seed has an energy of ~10 nJ with 3–5% rms shot-to-shot noise.

After pulse retiming, the pump and seed are spatially overlapped with orthogonal polarization by reflecting the BBIR off a CaF_2 wire grid polarizer (Specac) which transmits the pump. The collinear pump and seed pulses are focused into a 1-mm GaSe crystal (z-cut, Eksma) using an Au-OAP (f = 200 mm). The crystal is placed 25 mm before the focus where pump and seed diameters are 1.6-mm and 0.5-mm 1/e^2 (yielding approximate Gaussian peak intensities 200 and 0.2 GW/cm^2), respectively. Type-1 phase matching in GaSe at a phase-matching angle (θ_{PM}) of 11.2–11.8° supports a broad bandwidth [Fig. 2(a)], producing amplified BBIR signal and idler with spectra displayed in Fig. 2(b). The amplified spectra exceed 1000 cm^{-1}, somewhat narrower than the seed due to phase matching. Parametric amplification with θ_{PM} = 11.2° yields a slope efficiency of 8% and 4% for signal and idler, respectively [Fig. 2(c)], and pulse energies of 6 μJ and 3 μJ (±1% rms) with a 105-μJ pump, consistent with the ~2:1 ratio of output frequencies. This represents a 20% total photon conversion efficiency considering the ~16% Fresnel reflection off the GaSe crystal, and the lack of saturation suggests further scalability. Spatial profiles of the collimated (focused) beams were measured by transmission through a 400 (100)-μm pinhole mounted on an x-y stage [Figs. S1 in Supplement 1 and 2(c) inset].

After recollimation to a diameter of 7-mm 1/e^2, the amplified BBIR is separated from the residual pump by reflection off a Si wafer at Brewster's angle, which transmits the horizontally polarized pump and reflects 72% of the amplified BBIR. This approach was chosen to minimize dispersion, and more efficiently transmit the pump compared to the polarizer used to combine the beams. The signal and idler exit the GaSe crystal at a small angle (<1°) with respect to each other due to refraction, which we use to separate the beams by passing one through a 200-μm pinhole at the focus of two matched Au-OAPs (f = 100 mm).

For pulse compression, minimizing the total transmissive material before the sample is an important design consideration. While group delay dispersion (GDD) can be compensated for in the MIR using oppositely signed GDD materials, third-order dispersion (TOD) is positive for all materials and grows rapidly with increasing wavelength [17]. The amplified BBIR pulse exits the OPA having transmitted through only the 1-mm GaSe crystal with GDD of 230 fs^2 at 3 μm. Considering also the 3-mm KBr beam splitter (51 fs^2) in the 2D IR interferometer used here (Fig. 1) suggests that the 3-μm signal can be compressed with 3 mm of CaF_2 (GDD = –318 fs^2), which is also a desirable material for sample windows [18]. Idler compression poses a greater practical challenge because of the large TOD from transmissive material at 6 μm and longer wavelengths.

Pulse compression was measured with frequency-resolved optical gating (FROG) [19] using the interferometer and spectrometer in Fig. 1 with slight modification (Fig. S2 in Supplement 1). A noncollinear pulse pair is generated in a Mach–Zehnder interferometer (MZI) with two 3-mm AR coated 50/50 KBr beam splitters. Signal (or idler) pulses are crossed in a 0.5-mm Si (or 1-mm Ge) window at the sample position using an Au-OAP (f = 100 mm) and one pulse is dispersed with a monochromator onto an HgCdTe (MCT) detector. The third-order non-resonant response is collected as a function of wavelength and interferometer delay. This measurement carries the same information as the transient grating FROG measurement [20,21], and is analyzed this way using commercial software (Femtosoft). The third-order FROG was chosen to avoid phase-matching limitations in second-order processes such as SHG FROG.

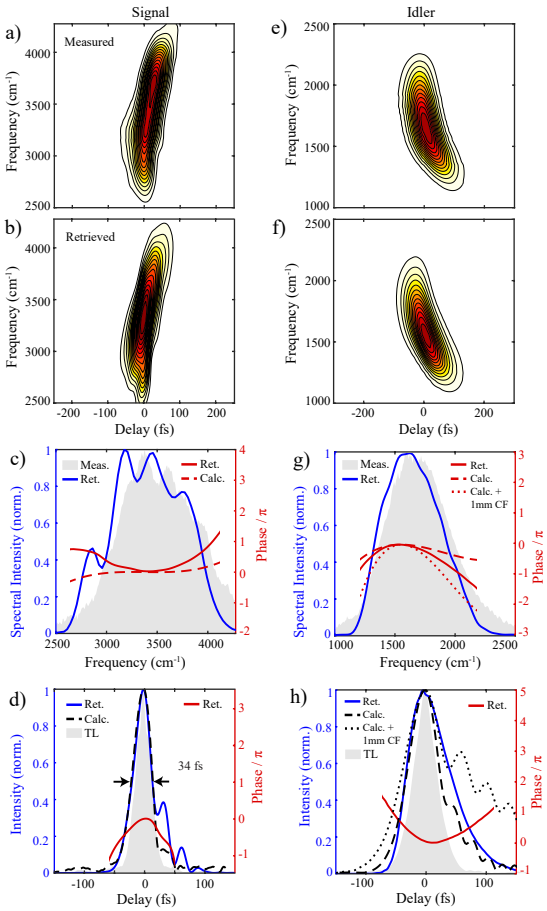

Fig. 3. FROG characterization of (a)–(d) signal using nonresonant response in 0.5 mm Si with 3 mm CaF_2 added in the beam path and (e)–(f) idler using 1 mm Ge. (a) and (e) Measured FROG spectrogram. (b) and (f) Retrieved spectrogram. (c) and (g) Retrieved spectral intensity (blue) and spectral phase (red), along with measured spectrum (shaded) and calculated spectral phase accounting for transmissive material in the beam (dashed) and addition of 1 mm CaF_2 (dotted). (d) and (h) Retrieved time-domain intensity (blue) and phase (red), along with the transform limit (shaded) and calculated intensity (dashed, dotted) from the measured spectrum and calculated spectral phases in panels (c) and (g).

Figure 3 displays the FROG measurements and retrievals for signal [Figs. 3(a)–3(d)] and idler [Figs. 3(e) and 3(f)]. For the signal characterization, 3 mm CaF_2 was placed before the MZI, which minimized the retrieved pulse width (Fig. S3 in Supplement 1). The retrieved pulse width was 34 fs FWHM, corresponding to <4 optical cycles at 3 μm; the transform limit was 26 fs. For comparison, the spectral phase was calculated accounting for the GDD and TOD of the GaSe, KBr, and CaF_2 material in the beam path [dashed line in Fig. 3(c)] using data from Ref. [22]. Together with the measured spectrum, the calculated spectral phase was used to model the pulse intensity in the time domain [dashed black line in Fig. 3(d)]. The residual positive GDD in the retrieved FROG is likely the result of the Si window used for characterization, as suggested by the calculated spectral phase when Si dispersion is neglected.

Idler FROG characterization [Figs. 3(e) and 3(f)] was measured without additional material in the beam path. The retrieved pulse width was 80 fs FWHM, due to uncompensated negative GDD in GaSe at 6 μm and positive TOD from GaSe and KBr; the transform limit was 40 fs. For comparison, the spectral phase was calculated accounting for 1 mm GaSe and 3 mm KBr (dashed line), with the addition of 1-mm CaF_2 (dotted line). This suggests that the GDD can be compensated by a material such as Ge with positive GDD, and that spectroscopic experiments will require an alternative to CaF_2 sample windows such as thin Si_3N_4 windows [23].

To demonstrate the utility of this light source for spectroscopy, 2D IR measurements were collected with the spectrometer in Fig. 1 using the compressed signal for excitation and detection. The detection pulse is a 1% reflection off a 1-mm CaF_2 wedge, and the excitation pulse pair exit the MZI collinearly. Pulses meet at the sample in the pump–probe geometry [25,26]. The nonlinear signal is measured as an absorption change in the frequency domain with a monochromator and MCT detector. For compression, 1 mm CaF_2 was added in the beam path before and after the wedge such that all beams pass through at total of 3 mm including the sample window. The instrument response function, measured in a 1-mm CaF_2 window, decays before 100 fs (Fig. S4 in Supplement 1).

The early-time 2D IR spectrum of isotopically dilute HOD in D_2O in the O-H stretch region (a benchmark that has been

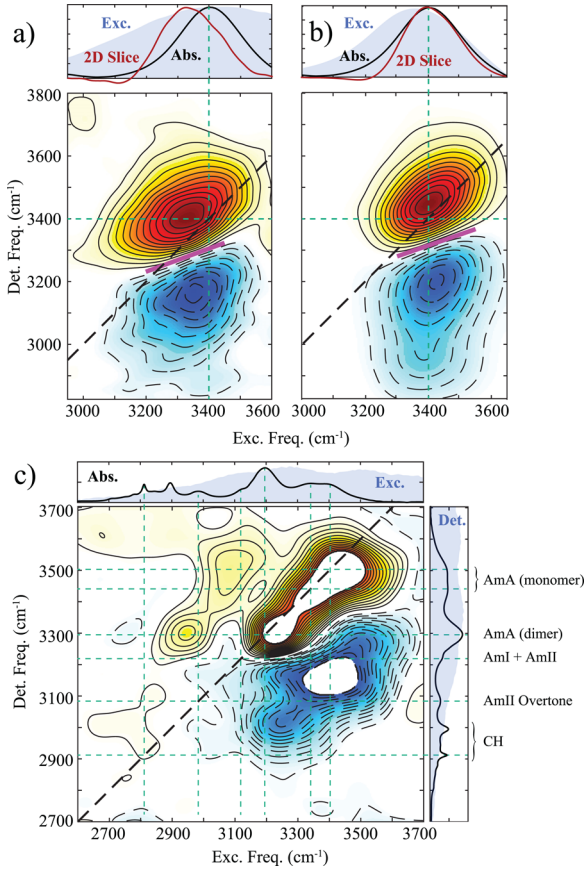

Fig. 4. 2D IR spectra of (a) and (b) 1% HOD in D_2O and (c) 1 M NMA in DMSO-d6, collected at $\tau_2 = 100$ fs with parallel polarization. Samples were excited with (a) and (c) the signal pulse reported in this work and (b) the 3-μm source described in Ref. [8]. Preliminary assignments in panel (c) are based on Ref. [24]. Color scheme: black, normalized linear absorption spectra; shaded, pulse spectra; red, diagonal 2D IR slice through the maximum; dashed green, selected transitions; magenta, nodal line.

studied both experimentally and theoretically [27,28]) demonstrates the improved capabilities for line shape measurements with broadband excitation [Fig. 4(a)] compared to excitation with 300-cm^{-1} bandwidth FWHM [Fig. 4(b)] generated in a $KNbO_3$ OPA [8]. With BBIR excitation, the 2D IR spectrum reproduces the fundamental (red) and excited-state absorption (ESA, blue) features, and quantitatively reproduces the nodal line slope [6]. Notably, broadband excitation reveals that the maximum of the O-H stretch in the 2D IR spectrum is red-shifted in excitation frequency relative to the linear absorption spectrum, which is not observed in Fig. 4(b) where the 2D IR line shape is artificially narrowed by the excitation bandwidth. This difference between the 2D IR and linear absorption peak positions is an expected result of the frequency-dependent transition dipole moment of the O-H stretch [28].

The 2D IR spectrum of N-methylacetamide (NMA) dimers in DMSO-d6 [Fig. 4(c)] demonstrates the capabilities of broadband excitation for cross peak measurements, simultaneously exciting features spanning 1000 cm^{-1}. This spectrum displays numerous resonances that arise from the coupled fundamental and overtone vibrations of the amide group [24]. The Amide A (AmA) fundamental appears at frequencies characteristic of both monomers and H-bonded dimers, while the rich cross peak structure arises from couplings to overtones and combination bands of Amide I and Amide II (AmI + AmII), which shift in frequency upon dimerization. Notably, uphill cross peaks can be observed simultaneously with diagonal features, which is necessary for quantitative comparison.

In summary, we report a source for broadband, multi-μJ MIR pulses centered at 3 μm and 6 μm and illustrate 2D IR spectroscopy with broadband excitation using the signal pulse. This source can be applied between 1000 and 4000 cm^{-1} covering the vibrational fingerprint region, making it particularly useful for broad resonances such as O-H and N-H vibrations in aqueous solutions. The gain curve of the OPA is not saturated, suggesting further energy scalability with increased pump energy or crystal length, though tradeoffs with self-phase modulation or reduced phase-matching bandwidth may arise. With future work to independently manipulate, compress, and combine signal and idler, we envision broad bandwidth 2D IR spectroscopy that measures time-resolved vibrational correlations simultaneously across the entire mid-infrared spectrum.

Funding. Office of Basic Energy Sciences, U.S. Department of Energy (DE-SC0014305).

Acknowledgments. We thank Bogdan Dereka for technical support. This work was supported by the Office of Basic Energy Sciences, U.S. Department of Energy, under Grant No. DE-SC0014305.

Disclosures. The authors declare no conflicts of interest.

Data availability. Data may be obtained from the authors upon reasonable request.

Supplemental document. See Supplement 1 for supporting content.

REFERENCES

1. H. Liang, P. Krogen, Z. Wang, H. Park, T. Kroh, K. Zawilski, P. Schunemann, J. Moses, L. F. Dimauro, F. X. Kärtner, and K. H. Hong, Nat. Commun. **8**, 1 (2017).
2. A. D. Koulouklidis, C. Gollner, V. Shumakova, V. Y. Fedorov, A. Pugžlys, A. Baltuška, and S. Tzortzakis, Nat. Commun. **11**, 292 (2020).
3. G. Herink, D. R. Solli, M. Gulde, and C. Ropers, Nature **483**, 190 (2012).
4. A. M. Stingel and P. B. Petersen, J. Phys. Chem. B **120**, 10768 (2016).
5. K. Tian, L. He, X. Yang, and H. Liang, Photonics **8**, 437 (2021).
6. P. Hamm and M. Zanni, (Cambridge University Press, 2011).
7. R. A. Kaindl, M. Wurm, K. Reimann, P. Hamm, A. M. Weiner, and M. Woerner, J. Opt. Soc. Am. B **17**, 2086 (2000).
8. C. J. Fecko, J. J. Loparo, and A. Tokmakoff, Opt. Commun. **241**, 521 (2004).
9. J. A. Fournier, W. B. Carpenter, N. H. C. Lewis, and A. Tokmakoff, Nat. Chem. **10**, 932 (2018).
10. T. Fuji and Y. Nomura, Appl. Sci. **3**, 122 (2013).
11. P. B. Petersen and A. Tokmakoff, Opt. Lett. **35**, 1962 (2010).
12. L. von Grafenstein, M. Bock, D. Ueberschaer, K. Zawilski, P. Schunemann, U. Griebner, and T. Elsaesser, Opt. Lett. **42**, 3796 (2017).
13. K. Liu, H. Liang, L. Wang, S. Qu, T. Lang, H. Li, Q. J. Wang, and Y. Zhang, Opt. Lett. **44**, 1003 (2019).
14. R. Budriūnas, K. Jurkus, M. Vengris, and A. Varanavičius, Opt. Express **30**, 13009 (2022).
15. C. Gaida, M. Gebhardt, T. Heuermann, F. Stutzki, C. Jauregui, J. Antonio-Lopez, A. Schülzgen, R. Amezcua-Correa, A. Tünnermann, I. Pupeza, and J. Limpert, Light: Sci. Appl. **7**, 94 (2018).
16. S. Vasilyev, I. S. Moskalev, V. O. Smolski, J. M. Peppers, M. Mirov, A. V. Muraviev, K. Zawilski, P. G. Schunemann, S. B. Mirov, K. L. Vodopyanov, and V. P. Gapontsev, Optica **6**, 111 (2019).
17. N. Demirdöven, M. Khalil, O. Golonzka, and A. Tokmakoff, Opt. Lett. **27**, 433 (2002).
18. T. G. Mayerhofer, S. Pahlow, U. Hubner, and J. Popp, Anal. Chem. **92**, 9024 (2020).
19. R. Trebino, K. W. DeLong, D. N. Fittinghoff, J. N. Sweetser, M. A. Krumbügel, B. A. Richman, and D. J. Kane, Rev. Sci. Instrum. **68**, 3277 (1997).
20. T. Joo, Y. Jia, J. Y. Yu, M. J. Lang, and G. R. Fleming, J. Chem. Phys. **104**, 6089 (1996).
21. J. A. Gardecki, S. Constantine, Y. Zhou, and L. D. Ziegler, J. Opt. Soc. Am. B **17**, 652 (2000).
22. W. J. Tropf, M. E. Thomas, and T. J. Harris, 2nd ed., M. Bass ed., (McGraw-Hill, 1995), p. 33.3.
23. A. Kundu, F. Dahms, B. P. Fingerhut, E. T. J. Nibbering, E. Pines, and T. Elsaesser, J. Phys. Chem. Lett. **10**, 2287 (2019).
24. L. De Marco, M. Thämer, M. Reppert, and A. Tokmakoff, J. Chem. Phys. **141**, 034502 (2014).
25. L. P. DeFlores, R. A. Nicodemus, and A. Tokmakoff, Opt. Lett. **32**, 2966 (2007).
26. L. De Marco, "The Molecular Dynamics of Hydrogen-Bonding Explored with Broadband Two Dimensional Infrared Spectroscopy," Ph.D thesis (Massachusetts Institute of Technology, Department of Chemistry, 2016).
27. L. De Marco, K. Ramasesha, and A. Tokmakoff, J. Phys. Chem. B **117**, 15319 (2013).
28. B. Auer, R. Kumar, J. R. Schmidt, and J. L. Skinner, Proc. Natl. Acad. Sci. U. S. A. **104**, 14215 (2007).